HHS Public Access

Author manuscript

Adv Mater. Author manuscript; available in PMC 2017 January 27.

Published in final edited form as:

Adv Mater. 2016 January 27; 28(4): 677–684. doi:10.1002/adma.201503310.

Microfluidic bioprinting of heterogeneous 3D tissue constructs using low viscosity bioink

Dr. Cristina Colosi,
Biomaterials Innovation Research Center, Brigham and Women's Hospital, Harvard Medical School. Cambridge, MA, USA. 02139

Harvard-MIT Division of Health Sciences and Technology. Cambridge, MA, USA. 02139

Department of Chemistry, Sapienza Università di Roma. Piazzale Aldo Moro 5, Rome, Italy. 00185

Dr. Su Ryon Shin,
Biomaterials Innovation Research Center, Brigham and Women's Hospital, Harvard Medical School. Cambridge, MA, USA. 02139

Harvard-MIT Division of Health Sciences and Technology. Cambridge, MA, USA. 02139

Wyss Institute for Biologically Inspired Engineering. Boston, MA, USA. 02115

Vijayan Manoharan,
Biomaterials Innovation Research Center, Brigham and Women's Hospital, Harvard Medical School. Cambridge, MA, USA. 02139

Harvard-MIT Division of Health Sciences and Technology. Cambridge, MA, USA. 02139

Dr. Solange Massa,
Biomaterials Innovation Research Center, Brigham and Women's Hospital, Harvard Medical School. Cambridge, MA, USA. 02139

Harvard-MIT Division of Health Sciences and Technology. Cambridge, MA, USA. 02139

Programa de Doctorado en Biomedicina, Universidad de los Andes. Santiago, Chile. 7620001

Dr. Marco Costantini,
Department of Chemistry, Sapienza Università di Roma. Piazzale Aldo Moro 5, Rome, Italy. 00185

Dr. Andrea Barbetta,
Department of Chemistry, Sapienza Università di Roma. Piazzale Aldo Moro 5, Rome, Italy. 00185

Dr. Mehmet Remzi Dokmeci,
Biomaterials Innovation Research Center, Brigham and Women's Hospital, Harvard Medical School. Cambridge, MA, USA. 02139

Harvard-MIT Division of Health Sciences and Technology. Cambridge, MA, USA. 02139

*These authors contributed equally as corresponding author to this work.

Wyss Institute for Biologically Inspired Engineering. Boston, MA, USA. 02115

Mariella Dentini* **[Prof.]**, and
Department of Chemistry, Sapienza Università di Roma. Piazzale Aldo Moro 5, Rome, Italy. 00185

Ali Khademhosseini* **[Prof.]**
Biomaterials Innovation Research Center, Brigham and Women's Hospital, Harvard Medical School. Cambridge, MA, USA. 02139

Harvard-MIT Division of Health Sciences and Technology. Cambridge, MA, USA. 02139

Wyss Institute for Biologically Inspired Engineering. Boston, MA, USA. 02115

College of Animal Bioscience and Technology, Department of Bioindustrial Technologies, Konkuk University, Hwayang-dong, Kwangjin-gu, Seoul 143-701, Republic of Korea

Department of Physics, King Abdulaziz University, Jeddah 21569, Saudi Arabia

Keywords

Bioprinting; Cell-laden bioink; 3D Tissue engineering; Vascular tissue engineering; Microfluidics

Three-dimensional (3D) functional tissue constructs with tailored biological and mechanical properties are needed in regenerative medicine and tissue engineering [1]. However, the development of highly organized and functional 3D tissue constructs remains an unsolved challenge. Recapitulating *in vitro* the 3D hierarchical microarchitecture comprising multiple cell types and extracellular matrix (ECM) components of native tissues revealed a difficult target[2]. In such a context, bioprinting emerged as a technology with the potential to create 3D tissue constructs endowed with *in vivo* like biological function compared to conventional microfabrication strategies such as micromolding, biotextiles, and photolithography[3]. Bioprinting allows for the precise positioning of cellularized structures on demand, either embedded in hydrogels or free from scaffold support. In the past, researchers have tried to employ different technologies for deposition and patterning of bioinks in 3D printing such as microextrusion [4, 5], inkject [6], magnetic [7] and laser printing [8]. The technology has also adressed biological needs like the printing of cartilage[9] and celullarized structures with succesuful results meeting both printing resolution and cell requirements[10]. Despite all significant advances in 3D bioprinting, the precise positioning/switching of different cell-types and biomaterials to create multicellular 3D structures that resemble the physical properties of *in vivo* environments still remains one of the major challenges.

To address these challenges, we present a novel bioprinting paradigm that a) enables simultaneous multimaterial deposition, b) allows the creation of a viable 3D cell-laden construct, c) uses bioinks formulations that induce the spreading and migration of embedded cells, and d) allows for the post-seeding of an additional cell type on top of the bioprinted scaffold. Previously, Gao et al [11] introduced a fast coaxial extrusion system as a nutrient delivery method for cells while othes choose to combine bioinks to observe cell proliferation[12]. Recenlty, another microfluidic printhead combined with a 3D printing system was introduced. The technique shows two PDMS viscoelastic inks extruding from a

single nozzle, solving the setback of aligment in slow multiple nozzles bioprinting systems [13]. Therefore, multimaterial deposition can be achieved by utilizing the microfluidic platform incorporated to 3D printing system. However, some of the previously mentioned techniques showed lack of resolution[12], limited cell viablity[11] and limited tissue versatility[9] compared to our system. This kind of 3D printing system has not been established before with cell-laden bioinks to create multicomponent/multicellular tissue constructs with this level of definition and celullar behavior. In particular, it is anticipated that advances in biomaterials are required to enable printing low viscosity materials with enhanced biological properties that will enhance the resulting tissue funtion.

Cell responsive bioink that allows spreading and migration of the cells, and at the same time, have a low viscosity and fast gelation process is a critical requirement while developing microfluidic-3D bioprinting system. It also needs to offer an adequate mechanical support for the cells located inside and outside of the bioprinted scaffold[14]. The low viscoscous bioink allows the use a thinner nozzle and increases the dispensing speed which results in a higher printing resolution and decreasing fabrication time. It is also ideal for high density cell loading (10^7 cells/ml) within the polymeric solution that can be rapidly deposited reducing possible shear stress on the cells during the deposition step. In addition, this bioink goes through a fast gelation process generating shape fixation to create thick constructs with high cell viability during spending process. With these properties, the bioink can be dispensed through a microfluidic-based extrusion system to rapidly and precisely switch between different bioinks and patterns[15, 16]. Therefore, the integration of 3D bioprinting with microfluidic platforms can allow the creation of heterogeneous 3D viable structures with a new level of definition and efficiency.

Previously, we have shown that by using a coaxial extrusion system and a 3D printer, a multi-layered scaffold can be obtained starting from a liquid solution of alginate[17]. This method relies on the property of alginate solutions to undergo an instantaneous gelation when exposed to calcium ions[18]. The simultaneous extrusion of an alginate and a calcium ion solutions through the inner and outer needles, respectively, of the coaxial extruder permits the formation of a gel fiber at the tip of the dispensing system that is layered according to any pre-determined design by the 3D printer. Despite its simplicity, this dispensing system addresses multiple problems encountered in the bioprinting practice. For instance, it is possible to print low viscous bioinks with excellent resolution using a biocompatible crosslinking method, obtaining macroscopic, porous 3D structures with single fiber thickness of the order of one hundred micrometers. Furthermore, the chemical formulation of the printing solution can be designed to provide an optimal microenvironment for the embedded cells by combining alginate with other stable gel-forming cell responsive biopolymers. Alginate can be easily dissolved in the absence of calcium ions, do not have cell binding sites, and provide a controllable biodegradability. The concentration and crosslinking densities of the two different hydrogel-precursor polymers are respectively adjusted to enable a higher 3D printing resolution of cell laden fibers to recreate the ideal microenvironment cell spreading and organization.

Here, we addressed the above mentioned challenges by developing a low viscosity bioink by using a blend of alginate and gelatin methacroyl (GelMA). GelMA is used for cell-

encapsulation due to its ability to form a chemically stable hydrogel when exposed to light compared to ionic crosslinked alginate [19]. GelMA also shows a great bioactivity attributable to its abundance of integrin-binding motifs and matrix metalloproteinase sensitive group which promoted cells adhesion and cellular migration within GelMA matrix [20]. It has been demonstrated that low concentrations of GelMA hydrogels (< 5% w/v GelMA) with a low degree of acryloyl modification show spontaneous organization of encapsulated cells such as human mesenchymal stem cells (hMSC) and endothelial cells compared to the high concentration (>10% w/v GelMA) and/or high degree of acryloyl modification of GelMA [21]. Therefore, we hypothesized that GelMA at low concentrations could be a suitable material to be used as a bioink. However, printing uniform and stacked cell-laden fibers using low concentrations of GelMA (< 20% w/v GelMA) [22] was found to be challenging, resulting in the deposition of strands that spread out on the surface. The use of the dispensing system described in this work allows overcoming problems associated with printability of low concentrations GelMA solutions. Physically crosslinked alginate fibers acted as structural template maintaining the printed multi-layer constructs without collapsing (Figure 1a). After printing, GelMA contained in the cell-laden microfibers was covalently crosslinked by exposition to UV light (Figure 1b). This process guarantees bonding at the areas of contact among fibers belonging to adjacent layers and determined the overall mechanical properties of the scaffolds. In the same fashion, other bioinks including photocrosslinkable biomaterials, such as hyaluronic acid[23] and elastin [24]methacryloyl can be printed with the described deposition strategy.

The bioprinting step was performed using a coaxial-needle extrusion system, in which the bioink mixture containing: alginate, GelMA, photoinitiator, and cells, was designed to flow in the internal needle (27G, Diameter: 210 μm) while the ionic crosslinking solution ($CaCl_2$), was designed to flow through the external needle (19G, Diameter: 690 μm)[25]. When the ionic crosslinking solution came in contact with the bioink mixture, the alginate was ionically crosslinked resulting in hydrogel microfibers (Figure 1c). In order to find out the optimal printing condition, we used a fixed concentration of GelMA (4.5% w/v) and varied those of alginate (from 1.0 to 4.0% w/v) and $CaCl_2$ (from 0.3 to 0.6M) and printing tests were carried out systematically. We used a low-molecular weight alginate (33 kDa) to obtain a bioink with low viscosity. As displayed in Figure 1d, the printability of the bioink was achieved by increasing the concentration of alginate and decreasing the concentration of the $CaCl_2$ solution. In order to avoid cell death we kept a low concentration of $CaCl_2$. Thus, the optimal formulation was represented by 4% w/v alginate and a 0.3M solution of $CaCl_2$. We then optimized the composition of the bioink's solvent to match the physiological conditions of neutral pH and iso-osmolarity. Water, HEPES (25mM, pH 7.4), and HEPES/ Fetal Bovine Serum (FBS, 10% v/v) were used as solvents for the alginate (4%) / GelMA (4.5%) formulations. This mixture was printed with a crosslinking solution containing 0.3M $CaCl_2$, 25mM HEPES and 10% FBS. These conditions guaranteed 80% viability (Figure S1).

To confirm the low viscosity of the bioink, rheological properties of GelMA, alginate, and alginate/GelMA mixture were measured (Figure 1e). The viscosity of alginate/GelMA mixture was found to be three times higher than that of pure alginate. However, the solution exhibited lower viscosity values (0.08 Pa/sec) compared to previous studies with a

decellularized ECM bioink (2.8 – 23.6 Pa/sec) [26, 27]. The presence of alginate also prevents the spontaneous thermal gelation of GelMA, so that the bioink maintains its low viscosity for prolonged periods of time at room temperature. Furthermore, the bioink exhibits a Newtonian behavior in the studied range of shear rate which allows the adjustment of the deposition speed without causing a reduction in the resolution of the printing process. In Figure 1f, the diameter of the printed microfiber was modified by changing the deposition speed while keeping constant the volumetric flow rate (5μl/min) of the bioink and crosslinking solution. The resultant diameter of printed fibers was between ~300 μm (for a deposition speed of 1 mm/sec) and ~150μm (for a deposition speed of 6 mm/sec). In addition, the optimized $CaCl_2$ (0.3M) concentration can prevent slippery behavior of the deposited layers during printing process. In this study, the structure tended to collapse with low concentrations (<0.3M) of $CaCl_2$ while high concentrations (>0.3M) of $CaCl_2$ produced slippery sets of fibers that compromised the structure's integrity preventing us from mobilizing it. Therefore, the optimal concentration (0.3M) of $CaCl_2$ enables us to stack multiple layers avoiding the aforementioned problems. However, the adhesion between layers was quickly reversible in a cell medium environment. UV light was then used to create covalent bonding between the different layers which can prevent the disintegration of the structure in a liquid medium. To confirm the robustness of the deposition technique in the production of larger structures, we printed a 3D open porous construct composed of 30 layers (3mm in height, 0–90° square grid, 150μm fiber diameter, 200μm fiber spacing, printing time: ~ 10 minutes) (Figure 1g). μCT was then used to evaluate 3D printed structure. The μCT rendered 3D reconstructions (Figure 1h) show a fully interconnected mesh formed by deposited fibers that can be stacked without signs of vertical collapse. In addition, the $CaCl_2$ solution kept the constructs moist during the deposition of microfiber enabling the stacking of multiple layers without causing any shrinkage of the deposited layers. Other techniques, though clever and ingenious, present uneven fibers that make difficult the creation of multi-layer stacked constructs due to their softness[28] while others struggle with definition and rigidity of the fiber[27]. Here we succeeded in printing thick, well defined and uniform constructs with a bioink suitable for tissue engineering applications.

To illustrate the possibility of generating multicomponent/multicellular tissue constructs we integrated a microfluidic system to our bioprinting set-up which allowed the rapid printing of bio-constructs formed by different materials to replicate the heterogeneity of native tissues. In previous studies, these kinds of heterogeneous structures have been created using multi-head systems[13]. However, they are relatively slow, which limits their use for cell-laden construct fabrication. Also, a microfluidic printhead combined with a 3D printing system was recently intrudced using only viscoelastic PDMS ink as opposed to cell-laden bioink[4]. Therefore, using microfluidics technology, the flow of different bioinks can be controlled integrating multi materials into fibers or droplets containing different cell types or even ECM components [15, 16]. During the deposition, the microfluidic channel can rapidly switch between different bioinks in a fully programmable manner where the bioink is dispensed using a single extruder. To carry this out we coupled the coaxial needles with a simple microfluidic chip with "Y" shaped channels and used two distinct bioinks having green and red fluorescent beads (Figure 2a). By selecting the type of bioink sent to the

extruder, we performed a serial coding of the two solutions and deposited heterogeneous structures containing different bioinks in different layers of the structure, as shown in Figure 2b,c–e. Alternatively, when the two bioinks flow simultaneously inside the extrusion system they produce a heterogeneous fiber containing two bioinks in a predetermined parallel pattern, as shown in Figure 2d, f–i. This integrated bioprinting-microfluidic technique opens new routes for the creation of complex and heterogeneous tissue fibers on demand.

We then introduced umbilical vein endothelial cells (HUVECs) into the bioink solution and observed levels of cellular viability, proliferation, and elongation. To assess cell viability within printed fibers using different UV crosslinking times, a live & dead assay was performed on day 3 after printing (Figure 3a, Figure S2). General loss of cell viability in printed constructs may occur due to stress during the encapsulation and printing procedure, free radicals produced by the photoinitiator, long UV exposure time, high stiffness of the crosslinked material or oxygen and nutrient limitations due to low molecular diffusion. However, in our photocrosslinking method, no significant cell viability loss was observed with UV light at a low intensity (6 mW/cm2 or 4 mW/cm2) for several minutes.[29] Therefore, the longer exposure times up to 30 sec to require for adequate crosslinking of printed constructs may not be able to decrease cell viability. Exposure times below 30 seconds for an adequate crosslinking process of the printed constructs do not decrease cell viability. However, prolonged UV exposure time (> 30 sec) significantly decreased cell viability. This is due to surplus free radicals and physical constraints of the stiff and closely crosslinked hydrogel network.[30] Generally, cell viability, proliferation and migration is limited within highly-crosslinked and stiff 3D hydrogel environments.[21, 31, 32] We then evaluated cell viability of the total construct (10 layers) at a fixed 30 seconds UV exposure 5 days after the printing process in different parts of the construct: top (Figure 3b), middle (Figure 3c), and bottom (Figure 3d). Each part of the structure was approximately 330 μm thick and could only be accessed through confocal microscopy. As shown in Figure 3e, the three different regions of the same construct exhibited an overall ~75% viability without significant difference between the different sections.

3D cell encapsulation has a number of advantages over 2D conventional cell culture that include improved cell-cell contacts and cell-matrix interactions[33]. These encapsulation techniques depend on the properties of the hydrogels defining the mechanical and chemical environment surrounding the cells [34]. In this case, the use of two independently crosslinkable hydrogels allow the tuning of mechanical properties of the cell-laden fibers to mimic the morphological and mechanical features of native tissue inducing cell spreading. In particular, we investigate how the UV crosslinking times of GelMA affected cell spreading and morphology 10 days after the printing. We used HUVECs as cellular model to illustrate the relation between the stiffness of construct and the spreading of the bioprinted cells. The encapsulated HUVECs exposed to a UV crosslinking time of 30 seconds showed improved cell spreading and organization compared to the constructs exposed for 15 sec. (Figure 3f–g). Interestingly, cells embedded in the printed constructs exposed to shorter UV crosslinking times (< 25sec) retained a spherical shape after 10 days of culture (Figure 3f, Figure S3). We conclude that the HUVECs need a determined stiffness to acquire proper morphology and organization within the 3D matrix. To confirm this hypothesis, unconfined compression tests were performed with acellular bulk structures swollen in DPBS at room

temperature. The elastic modulus of the hydrogels were found to increase as the UV exposure times were increased, which ranged from ~15kPa to ~55kPa (Figure 3h). Although it is known that cells tend not to spread when they are encapsulated in structures exhibiting elastic modulus over 25kPa, 15kPa is not stiff enough for the cells to attach and spread naturally. These observations are expected since the mechanical properties of the scaffold affect cell behavior such as proliferation, spreading, and migration [15, 35].

Cell-cell contact in an engineered environment is highly desired and also determines the ability of the material to promote *in vivo* like structures. To examine in detail the development of HUVECs within the construct, top view fluorescent images of bioprinted GFP-HUVECs structures were obtained at multiple time points (day 3, 5, 7, and 10), as shown in Figure S4a. By introducing the 'variance' filter in ImageJ across the images, the neighbor signal of each cell is lowered by reducing the noise and delivering a clear location of the cells, as shown in Figure S4b. In Figure S4b, at day 3 and 5 after printing, most of the cells showed a rounded shape and are located in the middle of the fiber (blue arrows). After day 7, elongated cells are seen at the edges of the printed fibers, especially in proximity to the contact point among fibers of the different layers. Finally, we observed that the signal of the elongated GFP-HUVECs is extensively detected at the edge of the printed fibers (red arrows) on day 10. Cell proliferation, migration and morphogenesis depend on the physical properties of surrounding hydrogel defined by its porosity and stiffness [21, 36] Alginate ionically cross-linked by Ca2+ dissolves within crosslinked GelMA hydrogel in cell medium [37]. To confirm the disintegration of alginate, we printed acellular structures using a fluorescent-labelled alginate/GelMA bioink and took fluorescent pictures over a 10 day period. Figure S5 showed that most of fluorescent-labelled alginate abandoned the printed construct by day 5. This could increase the porosity of hydrogel allowing cell migration to the edges of each fiber.[38] Furthermore, the crosslinked GelMA hydrogels permit cells to enzymatically degrade and remodel the hydrogel [32, 39] complementing the aforementioned process.

To confirm the HUVEC morphology in printed construct, we performed F-actin and DAPI staining. The organization of HUVECs within printed construct (10 layers) was analyzed by confocal microscopy after 10 days of culture and are shown in Figure 4b–d. In Figure 4b, the longitudinal and transversal cross-sections of the construct demonstrate a higher number of HUVECs at the edge of the fiber. As showed in Figure 4c the cells line up at edge of the fibers assuming a long-range architecture composed of a monolayer of cells. Interestingly, we observed perpendicular interconnected structures linking different levels of fiber layers (Figure 4d, Figure S6). Alignment of the cells in the periphery of the fibers is shown schematically in Figure 4a. In addition, we immunostained the construct to evaluate CD31 expression in the bioprinted HUVECs. CD31 is a membrane protein highly expressed on the membranes of endothelial cells and comprises a major chunk of the intercellular junction complexes[40]. Immunostaining of 10 day old 1 mm thick bioprinted HUVEC scaffold showed strong CD31 signal throughout the entire construct (Figure 4e–g). CD31 receptor signals (red) were located on the external part of the cell (Figure 4h) suggesting normal development of HUVECs along the printed structures.

Finally, to assess whether our construct could serve as an *in vitro* platform for cardiac tissue engineering applications, we decided to seed the scaffold structure with primary cardiomyocytes and creating a co-culture construct. For this purpose, freshly isolated neonatal rat cardiomyocytes were seeded on top of the a 10 day old bioprinted scaffold containing HUVEC cells. After 2 days in culture, the seeded cardiomyocytes showed synchronous beating in four different areas of the construct (Figures 4j, k). This demonstrated that our 3D bioprinted structure is soft enough for migration of HUVEC cells and is strong enough to support the synchronic beating of cardiomyocytes.

In conclusion, we developed a versatile 3D bioprinting technique and a novel bioink to produce highly viable and functional *in vitro* constructs with excellent resolution. The low viscosity alginate bioink creates a low resistance flow for a precise and controlled deposition by the microfluidic system. This enables the formation of complex heterogeneous structures using a single extruder system while the bioink can be easily tuned to the mechanical properties of the bioprinted constructs aimed to meet the requirements of specific tissues. Our alginate based bioink promoted cell migration and aligment within each fiber organizing the encapsulated cells. Remarkably, the 3D HUVEC scaffold also supported beating of primary cardiomyocytes indicating functionality and can possibly serve as scaffold for other cell types. The integration of our tailored bioink with a microfluidic platform in a 3D printing environment contributes to the creation of novel biomimetic heterogenous *in vitro* tissue models for regenerative medicine and drug discovery applications.

Supplementary Material

Refer to Web version on PubMed Central for supplementary material.

Acknowledgments

This work was supported by the Institute for Soldier Nanotechnology, National Institutes of Health (HL092836, EB02597, AR057837, HL099073), the National Science Foundation (DMR0847287), the Office of Naval Research Young Investigator award, ONR PECASE Award, a Discovery grant from National Sciences and Engineering Research Council of Canada and Università degli Study di Roma “La Sapienza” (Ateneo funds). Cristina Colosi thanks Università degli Study di Roma “La Sapienza” for a visiting PhD student fellowship c/o Harvard-MIT Division of Health Sciences and Technology. Authors also thank Project Management Institute Chile (PMI) together with Universidad de los Andes Chile (Programa de Doctorado en Biomedicina). Finally the authors acknowledge Mr. Gianfranco Angioni for generously donation low molecular weight alginate.

References

1. Dvir T, Timko BP, Kohane DS, Langer R. Nature nanotechnology. 2011; 6:13.
2. Atala A, Kasper FK, Mikos AG. Science translational medicine. 2012; 4:160rv12.
3. Murphy SV, Atala A. Nature biotechnology. 2014; 32:773.Wüst S, Müller R, Hofmann S. Journal of functional biomaterials. 2011; 2:119. [PubMed: 24956301] Melchels FPW, Domingos MAN, Klein TJ, Malda J, Bartolo PJ, Hutmacher DW. Progress in Polymer Science. 2012; 37:1079.
4. Hardin JO, Ober TJ, Valentine AD, Lewis JA. Advanced materials. 2015; 27:3279. [PubMed: 25885762]
5. Chang CC, Boland ED, Williams SK, Hoying JB. Journal of biomedical materials research. Part B, Applied biomaterials. 2011; 98:160.Duan B, Hockaday LA, Kang KH, Butcher JT. Journal of biomedical materials research. Part A. 2013; 101:1255. [PubMed: 23015540] Schuurman W, Khristov V, Pot MW, van Weeren PR, Dhert WJ, Malda J. Biofabrication. 2011; 3:021001. [PubMed: 21597163]

6. Xu T, Zhao W, Zhu JM, Albanna MZ, Yoo JJ, Atala A. Biomaterials. 2013; 34:130. [PubMed: 23063369] Cui X, Breitenkamp K, Finn MG, Lotz M, D'Lima DD. Tissue engineering. Part A. 2012; 18:1304. [PubMed: 22394017] Cui X, Boland T, D'Lima DD, Lotz MK. Recent patents on drug delivery & formulation. 2012; 6:149. [PubMed: 22436025] Christensen K, Xu C, Chai W, Zhang Z, Fu J, Huang Y. Biotechnology and bioengineering. 2015; 112:1047. [PubMed: 25421556]
7. Whatley BR, Li X, Zhang N, Wen X. Journal of biomedical materials research. Part A. 2014; 102:1537. [PubMed: 23666910]
8. Koch L, Gruene M, Unger C, Chichkov B. Current pharmaceutical biotechnology. 2013; 14:91. [PubMed: 23570054] Guillotin B, Souquet A, Catros S, Duocastella M, Pippenger B, Bellance S, Bareille R, Remy M, Bordenave L, Amedee J, Guillemot F. Biomaterials. 2010; 31:7250. [PubMed: 20580082] Michael S, Sorg H, Peck CT, Koch L, Deiwick A, Chichkov B, Vogt PM, Reimers K. PloS one. 2013; 8:e57741. [PubMed: 23469227]
9. Markstedt K, Mantas A, Tournier I, Martinez Avila H, Hagg D, Gatenholm P. Biomacromolecules. 2015; 16:1489. [PubMed: 25806996]
10. Hong S, Sycks D, Chan HF, Lin S, Lopez GP, Guilak F, Leong KW, Zhao X. Advanced Materials. 2015; 27:4035. [PubMed: 26033288]
11. Gao Q, He Y, Fu JZ, Liu A, Ma L. Biomaterials. 2015; 61:203. [PubMed: 26004235]
12. Ouyang L, Yao R, Chen X, Na J, Sun W. Biofabrication. 2015; 7:015010. [PubMed: 25691496]
13. Kolesky DB, Truby RL, Gladman AS, Busbee TA, Homan KA, Lewis JA. Advanced materials. 2014; 26:3124. [PubMed: 24550124] Jin-Hyung Shim J-SL, Kim Jong Young, Cho Dong-Woo. Journal of Micromechanics and Microengineering. 2012:22.
14. Skardal A, Atala A. Annals of biomedical engineering. 2014:1. [PubMed: 23918080] Malda J, Visser J, Melchels FP, Jüngst T, Hennink WE, Dhert WJA, Groll J, Hutmacher DW. Advanced Materials. 2013; 25:5011. [PubMed: 24038336] Rutz AL, Hyland KE, Jakus AE, Burghardt WR, Shah RN. Advanced Materials. 2015Arrigo M, Bettex D, Rudiger A. Critical care research and practice. 2014; 2014:840615. [PubMed: 24527212]
15. Onoe H, Okitsu T, Itou A, Kato-Negishi M, Gojo R, Kiriya D, Sato K, Miura S, Iwanaga S, Kuribayashi-Shigetomi K. Nature materials. 2013; 12:584. [PubMed: 23542870]
16. Brouzes E, Medkova M, Savenelli N, Marran D, Twardowski M, Hutchison JB, Rothberg JM, Link DR, Perrimon N, Samuels ML. Proceedings of the National Academy of Sciences. 2009; 106:14195.Yamada M, Utoh R, Ohashi K, Tatsumi K, Yamato M, Okano T, Seki M. Biomaterials. 2012; 33:8304. [PubMed: 22906609]
17. Colosi C, Costantini M, Latini R, Ciccarelli S, Stampella A, Barbetta A, Massimi M, Devirgiliis LC, Dentini M. J Mater Chem B. 2014; 2:6779.
18. Gregor ERM, Grant T, Rees David A, Smith Peter JC, Thom David. FEBS letters. 1973:32.Akbari M, Tamayol A, Laforte V, Annabi N, Najafabadi AH, Khademhosseini A, Juncker D. Adv Funct Mater. 2014; 24:4060. [PubMed: 25411576]
19. Kuo CK, Ma PX. Biomaterials. 2001; 22:511. [PubMed: 11219714]
20. Lee KY, Mooney DJ. Chemical reviews. 2001; 101:1869. [PubMed: 11710233] Aubin H, Nichol JW, Hutson CB, Bae H, Sieminski AL, Cropek DM, Akhyari P, Khademhosseini A. Biomaterials. 2010; 31:6941. [PubMed: 20638973] Ramón-Azcón J, Ahadian S, Obregón R, Camci-Unal G, Ostrovidov S, Hosseini V, Kaji H, Ino K, Shiku H, Khademhosseini A. Lab on a Chip. 2012; 12:2959. [PubMed: 22773042]
21. Nichol JW, Koshy ST, Bae H, Hwang CM, Yamanlar S, Khademhosseini A. Biomaterials. 2010; 31:5536. [PubMed: 20417964]
22. Bertassoni LE, Cardoso JC, Manoharan V, Cristino AL, Bhise NS, Araujo WA, Zorlutuna P, Vrana NE, Ghaemmaghami AM, Dokmeci MR, Khademhosseini A. Biofabrication. 2014; 6:024105. [PubMed: 24695367]
23. Khademhosseini A, Eng G, Yeh J, Fukuda J, Blumling J 3rd, Langer R, Burdick JA. Journal of biomedical materials research. Part A. 2006; 79:522. [PubMed: 16788972]
24. Annabi N, Mithieux SM, Zorlutuna P, Camci-Unal G, Weiss AS, Khademhosseini A. Biomaterials. 2013; 34:5496. [PubMed: 23639533]
25. Colosi C, Costantini M, Latini R, Ciccarelli S, Stampella A, Barbetta A, Massimi M, Devirgiliis LC, Dentini M. J. Mater. Chem. B. 2014; 2:13.

26. Malda J, Visser J, Melchels FP, Jungst T, Hennink WE, Dhert WJ, Groll J, Hutmacher DW. Advanced materials. 2013; 25:5011. [PubMed: 24038336]
27. Pati F, Jang J, Ha DH, Won Kim S, Rhie JW, Shim JH, Kim DH, Cho DW. Nat Commun. 2014; 5:3935. [PubMed: 24887553]
28. Kolesky DB, Truby RL, Gladman A, Busbee TA, Homan KA, Lewis JA. Advanced Materials. 2014; 26:3124. [PubMed: 24550124]
29. Fedorovich NE, Oudshoorn MH, van Geemen D, Hennink WE, Alblas J, Dhert WJ. Biomaterials. 2009; 30:344. [PubMed: 18930540]
30. Shin SR, Bae H, Cha JM, Mun JY, Chen Y-C, Tekin H, Shin H, Farshchi S, Dokmeci MR, Tang X, Khademhosseini A. ACS Nano. 2012; 6:362. [PubMed: 22117858]
31. Patel PN, Gobin AS, West JL, Patrick CW Jr. Tissue engineering. 2005; 11:1498. [PubMed: 16259604]
32. Hutson CB, Nichol JW, Aubin H, Bae H, Yamanlar S, Al-Haque S, Koshy ST, Khademhosseini A. Tissue engineering. Part A. 2011; 17:1713. [PubMed: 21306293]
33. Lee J, Cuddihy MJ, Kotov NA. Tissue Engineering Part B: Reviews. 2008; 14:61. [PubMed: 18454635]
34. Tibbitt MW, Anseth KS. Biotechnology and bioengineering. 2009; 103:655. [PubMed: 19472329]
35. Ehrbar M, Sala A, Lienemann P, Ranga A, Mosiewicz K, Bittermann A, Rizzi SC, Weber FE, Lutolf MP. Biophysical journal. 2011; 100:284. [PubMed: 21244824] Boontheekul T, Hill EE, Kong H-J, Mooney DJ. Tissue engineering. 2007; 13:1431. [PubMed: 17561804]
36. Patel PN, Gobin AS, West JL, Patrick CW Jr. Tissue Eng. 2005; 11:1498. [PubMed: 16259604] Engler AJ, Sen S, Sweeney HL, Discher DE. Cell. 2006; 126:677. [PubMed: 16923388] Hutson CB, Nichol JW, Aubin H, Bae H, Yamanlar S, Al-Haque S, Koshy ST, Khademhosseini A. Tissue Eng Part A. 2011; 17(13–14):1713. [PubMed: 21306293]
37. Akbari M, Tamayol A, Laforte V, Annabi N, Najafabadi AH, Khademhosseini A, Juncker D. Advanced Functional Materials. 2014; 24:4060. [PubMed: 25411576]
38. Tamayol A, Najafabadi AH, Aliakbarian B, Arab-Tehrany E, Akbari M, Annabi N, Juncker D, Khademhosseini A. Adv Healthc Mater. 2015
39. Koshy ST, Ferrante TC, Lewin SA, Mooney DJ. Biomaterials. 2014; 35:2477. [PubMed: 24345735]
40. Ayalon O, Sabanai H, Lampugnani M-G, Dejana E, Geiger B. The Journal of cell biology. 1994; 126:247. [PubMed: 8027182] DeLisser HM, Newman PJ, Albelda SM. Immunology today. 1994; 15:490. [PubMed: 7945775]

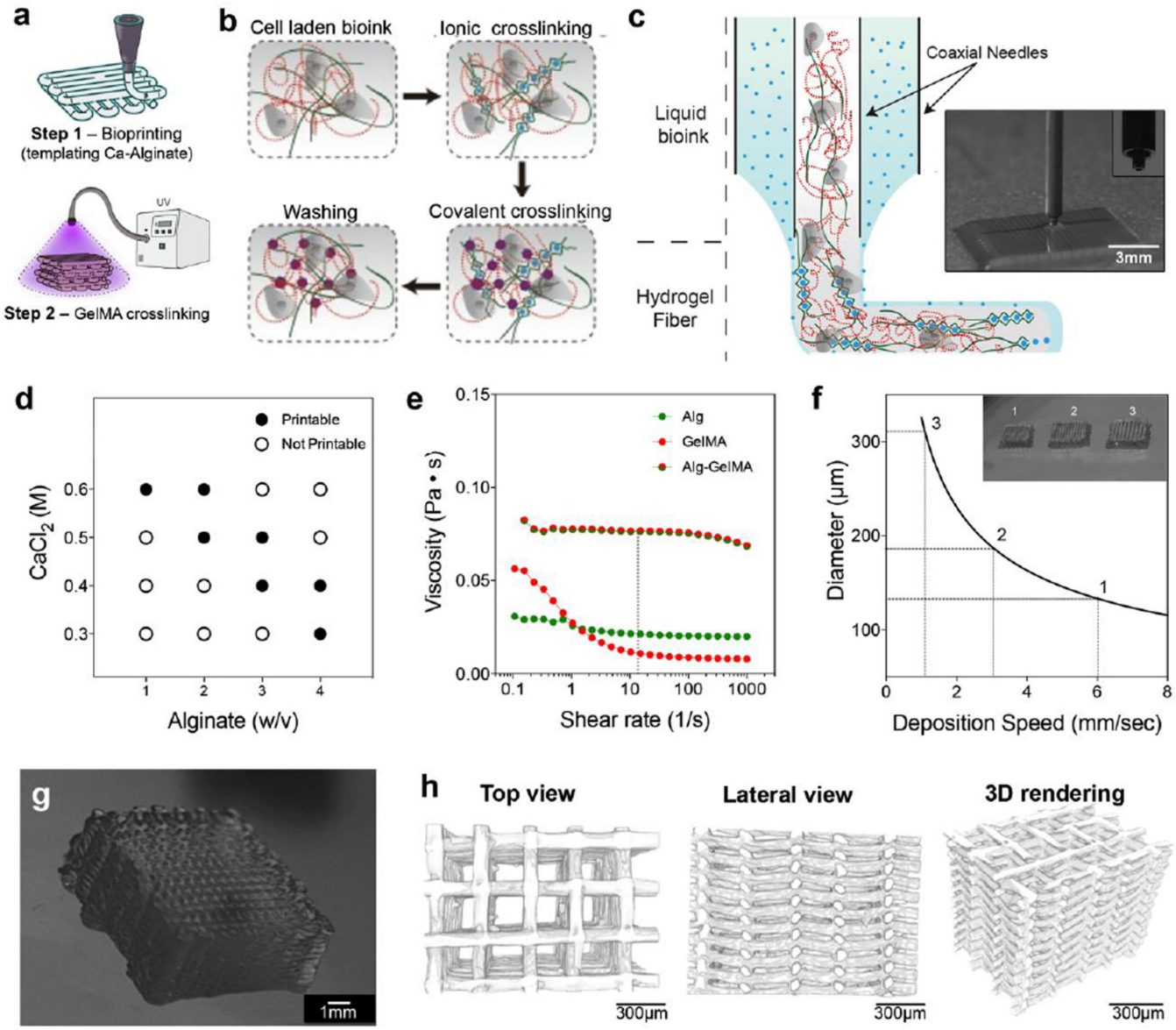

Figure 1.

(a) Schematic illustration of the layer-by-layer deposition based bioprinting technique consisting of two independent crosslinking steps. **(b, c)** The bioink contained GelMA (Red dashed lines), alginate (Green lines), photoinitiator and cells in the inner needle of the coaxial system. Simultaneously the $CaCl_2$ (blue dots) solution flows through the outer needle to induce the gelation of alginate chains. The construct was then UV crosslinked to solidify the GelMA prepolymer in the fiber. **(d)** Printability of different alginate concentrations and different $CaCl_2$ concentrations. GelMA concentration was kept constant (4.5% w/v). **(e)** Viscosities of alginate and GelMA and the combination of both at room temperature. **(f)** The fiber diameter varied with different deposition speeds, calculated for a bioink flow rate of 5μl/min. In the upper-right corner, photographs of the different fibers were obtained for deposition speeds of 6 mm/sec, 3 mm/sec, and 1mm/sec. **(g)** Photograph

of the final construct (30 layers). **(h)** Top, lateral and 3D μCT reconstructions of the final bioprinted 3D structure.

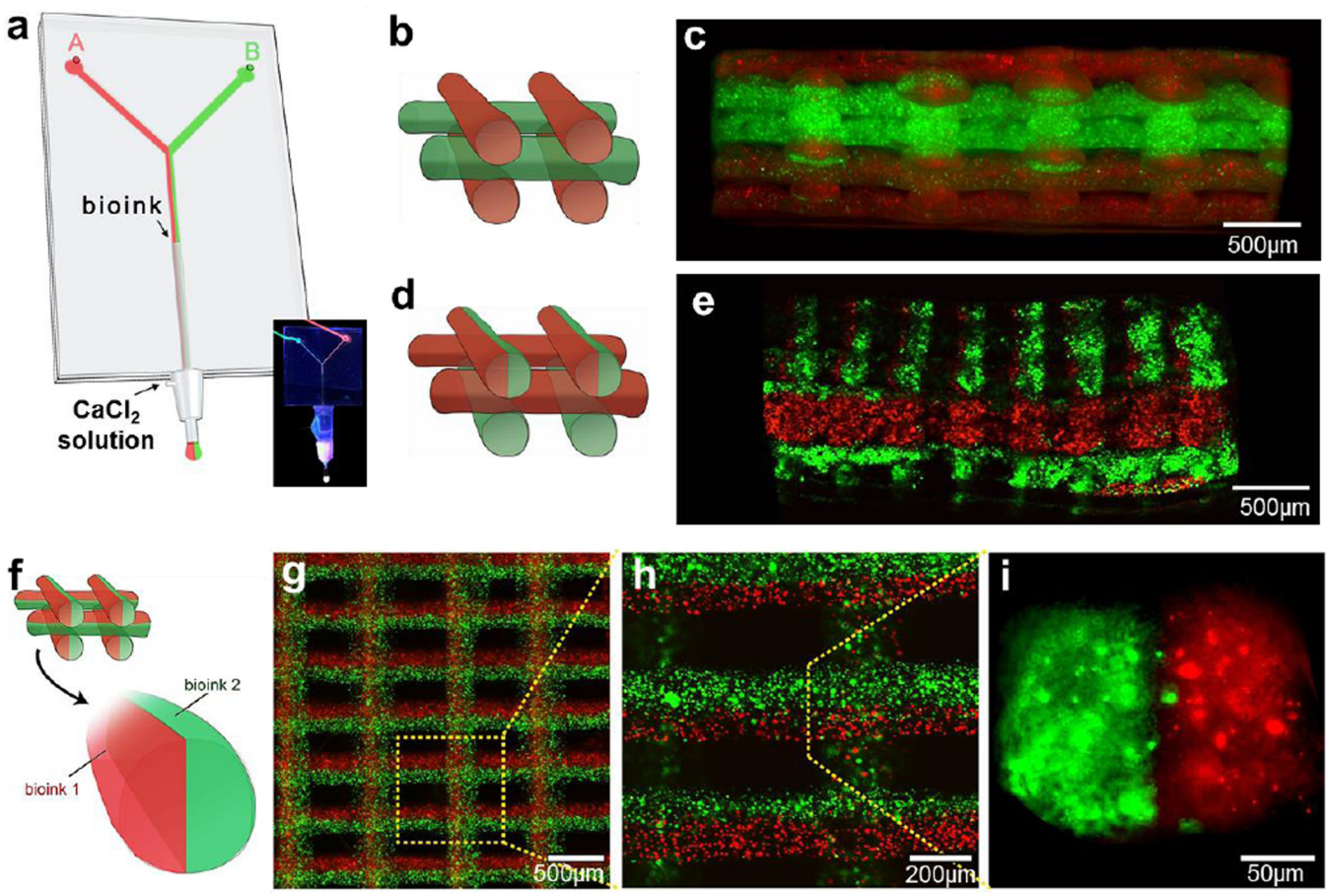

Figure 2.

(a) A microfluidic system was used to flow two separate bioinks containing red and green fluorescent beads that exited the device through a single extruder. Photograph (insert) of the coaxial needle system with a microfluidic chip with a “Y” shaped channel. The schematic diagram and fluorescence microscopy image of cross-section view of 3D construct with **(b and c)** alternative deposition, **(d and e)** alternative/simultaneous deposition, and **(f–i)** simultaneous deposition.

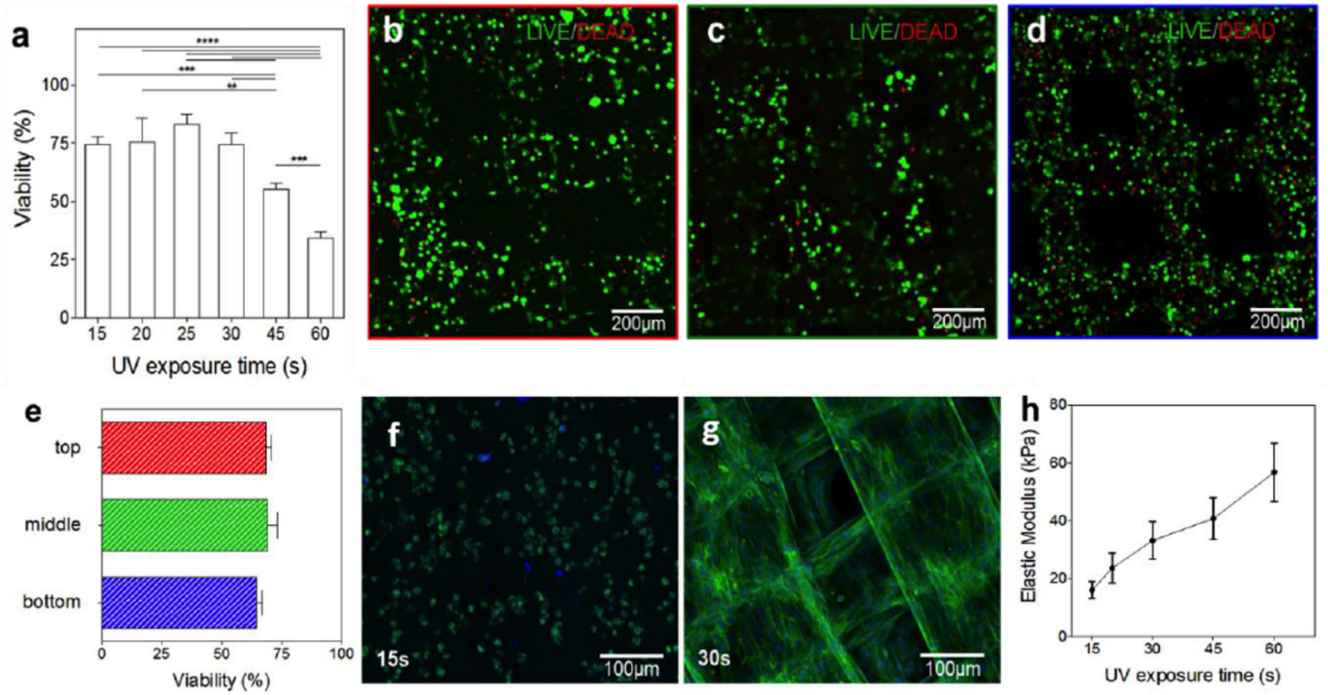

Figure 3.

(a) Viability of bioprinted HUVECs at day 3 as a function of different UV exposure times. **(b–d)** Confocal live-dead staining of bioprinted HUVECs at day 5. **(e)** Cell viability was assessed in the top **(b)**, middle **(c)** and bottom **(d)** of the construct. Confocal fluorescence F-actin and DAPI images of bioprinted HUVEC embedded construct with **(f)** 15 s and **(g)** 30s UV exposure time after 10 days in cell culture. **(h)** Elastic modulus of GelMA versus different UV exposure times.

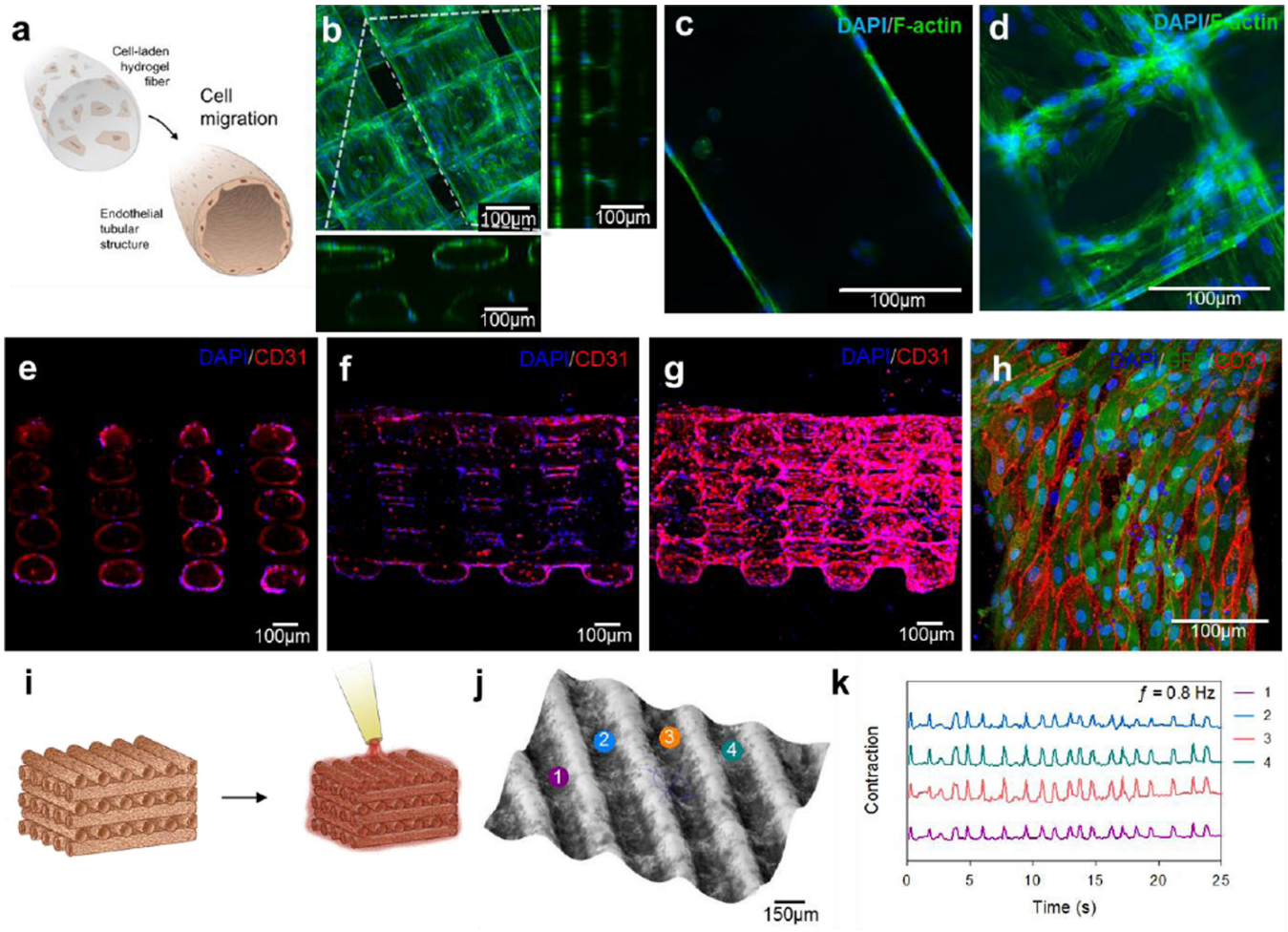

Figure 4.

(a) Schematic of the encapsulated HUVECs migrating to outer regions of the bioprinted fibers after 10 days of culture. Confocal microscopy images with **(b)** top view, **(c)** cross section view, and **(d)** fiber junctions showing interconnected structures. Confocal microscopy images of a 1mm thick construct that show a: **(e)** transversal cross-section, **(f)** longitudinal cross-section, **(g)** outer surface of the complete construct. **(h)** Top view of a single fiber immunostained for CD31 (red) and DAPI (blue). **(i)** Schematic illustration of the HUVEC structure before and after the cardiomyocyte seeding. **(j)** 3D surface plot of a microscopy image of the 3D HUVEC-cardiac tissue construct after two days of cardiomyocytes culture. **(k)** The beating rates of cardiomyocytes were monitored in four different zones (1, 2, 3, 4) of the construct which showed synchronous beating behavior.